Sidewall gratings in ultra-low-loss Si_3N_4 planar waveguides

Michael Belt,* **Jock Bovington, Renan Moreira, Jared F. Bauters, Martijn J. R. Heck, Jonathon S. Barton, John E. Bowers, and Daniel J. Blumenthal**

Electrical and Computer Engineering Department, University of California, Santa Barbara California 93106, USA
*michaelbelt@ece.ucsb.edu

Abstract: We demonstrate sidewall gratings in an ultra-low-loss Si_3N_4 planar waveguide platform. Through proper geometrical design we can achieve coupling constant values between 13 and 310 cm^{-1}. The TE waveguide propagation loss over the range of 1540 to 1570 nm is below 5.5 dB/m.

©2013 Optical Society of America

OCIS codes: (050.2770) Gratings; (230.7390) Waveguides, planar; (130.0130) Integrated optics.

References and links

1. L. A. Coldren, "Monolithic tunable diode lasers," IEEE J. Sel. Top. Quantum Electron. **12**(12), 988–999 (2000).
2. A. W. Fang, M. N. Sysak, B. R. Koch, R. Jones, E. Lively, Ying-Hao Kuo, Di Liang, O. Raday, and J. E. Bowers, "Single-wavelength silicon evanescent lasers," IEEE J. Sel. Top. Quantum Electron. **15**(3), 535–544 (2009).
3. D. Pastor, J. Capmany, D. Ortega, V. Tatay, and J. Marti, "Design of apodized linearly chirped fiber gratings for dispersion compensation," J. Lightwave Technol. **14**(11), 2581–2588 (1996).
4. A. Carballar, M. A. Muriel, and J. Azaña, "Fiber grating filter for WDM systems: an improved design," IEEE Photon. Technol. Lett. **11**(6), 694–696 (1999).
5. K. N. Nguyen, P. J. Skahan, J. M. Garcia, E. Lively, H. N. Poulsen, D. M. Baney, and D. J. Blumenthal, "Monolithically integrated dual-quadrature receiver on InP with 30 nm tunable local oscillator," Opt. Express **19**(26), B716–B721 (2011).
6. V. V. Wong, W. Y. Choi, J. M. Carter, C. G. Fonstad, H. I. Smith, Y. Chung, and N. Dagli, "Ridge-waveguide sidewall-grating distributed feedback structures fabricated by x-ray lithography," J. Vac. Sci. Technol. B **11**(6), 2621–2624 (1993).
7. J. T. Hastings, M. H. Lim, J. G. Goodberlet, and H. I. Smith, "Optical waveguides with apodized sidewall gratings via spatial-phase-locked electron-beam lithography," J. Vac. Sci. Technol. B **20**(6), 2753–2757 (2002).
8. E. H. Bernhardi, Q. Lu, H. A. G. M. van Wolferen, K. Wörhoff, R. M. de Ridder, and M. Pollnau, "Monolithic distributed Bragg reflector cavities in Al_2O_3 with quality factors exceeding 10^6," Photonics and Nanostructures – Fundamentals and Applications **9**(3), 225–234 (2011).
9. C. Lin, J. R. Adleman, E. W. Jacobs, J. S. Rodgers, R. Liang, T. Chen, and A. Fitting, "Higher order planar-waveguide Bragg grating on curved waveguide," in *Proceedings of the IEEE Photonics Conference*, (Arlington, VA, 2011).
10. T. E. Murphy, J. T. Hastings, and H. I. Smith, "Fabrication and characterization of narrow-band Bragg-refection filters in silicon-on-insulator ridge waveguides," J. Lightwave Technol. **19**(12), 1938–1942 (2001).
11. J. F. Bauters, M. J. R. Heck, D. D. John, J. S. Barton, C. M. Bruinink, A. Leinse, R. G. Heideman, D. J. Blumenthal, and J. E. Bowers, "Planar waveguides with less than 0.1 dB/m propagation loss fabricated with wafer bonding," Opt. Express **19**(24), 24090–24101 (2011).
12. A. Yariv and P. Yeh, *Photonics: Optical Electronics in Modern Communication* (Oxford, 2007), Chap. 12.
13. L. A. Coldren, S. W. Corzine, and M. L. Mašanović, *Diode Lasers and Photonic Integrated Circuits* (Wiley, 2012), Chap. 6.
14. K. O. Hill and G. Meltz, "Fiber Bragg grating technology fundamentals and overview," J. Lightwave Technol. **15**(8), 1263–1276 (1997).

1. Introduction

Bragg grating structures are an integral part of the diverse array of components that comprise an optical communications system. These include distributed tunable Bragg reflector (DBR) lasers [1], distributed feedback (DFB) lasers [2], dispersion compensators [3], and wavelength-division multiplexed (WDM) channel filters [4]. With the current push towards

#174182 - $15.00 USD Received 10 Aug 2012; revised 15 Sep 2012; accepted 19 Sep 2012; published 10 Jan 2013

coherent transmission and detection schemes [5], stable and extremely narrow linewidth lasers have become increasingly more important. A low loss grating capable of providing high reflectivity, while at the same time maintaining an extremely selective passband, is necessary to realize a new generation of coherent devices. Furthermore, low loss is critical in the scaling of large size photonic integrated circuits with stringent power requirements.

There have been prior results reported on sidewall grating technologies that include patterning through reactive-ion etching [6] and direct-write spatial-phase-locked electron-beam lithography [7]. Previous results in low loss, highly selective gratings include surface relief gratings integrated with aluminum oxide ridge waveguides [8] and sidewall gratings fabricated within a curved waveguide structure on a low loss silica platform [9]. Prominent results in these approaches have bandwidths on the order of 0.12 nm with coupling constant values of roughly 4.5 cm^{-1} [10]. The limitations to these approaches include their reliance on strict etch tolerances [8], as well as their requirements for multiple lithographic patterning and etch steps [6,10]. The limitations of prior approaches are primarily due to a combination of both design constraints and fabrication technology.

In this work we report for the first time the design and characterization of a collection of sidewall gratings in ultra-low-loss Si_3N_4 planar waveguides. Through simple design of waveguide geometry the presented sidewall gratings can achieve a wide range of coupling constants, including the possibility of the very low values required for an exceptionally narrow passband. Just as well, since the gratings are all defined in a single lithographic step, multiple types of gratings can follow one another along the same waveguide section. This creates an opportunity for integrated circuits with complex filter functions. The requirement of only a single lithography step means that the entire fabrication process becomes quite simple and highly tolerant.

2. Fabrication and grating structure

The silicon nitride waveguides are fabricated in a CMOS foundry using 248 nm stepper lithography on 200 mm silicon substrates. Figure 1(a) gives a schematic cross-section representation of the complete waveguide structure. Both the upper and lower thermal oxide claddings are 15 μm thick, while the low-pressure chemical vapor deposition (LPCVD) oxide is 3.1 μm thick. The 2.8 μm wide LPCVD Si_3N_4 waveguide core layer measures 100 nm in thickness. The complete waveguide fabrication process, including bonding steps, follows the work found in [11].

The TE waveguide propagation loss over the range of 1540 to 1570 nm monotonically decreased from 5.5 to 2.7 dB/m, as confirmed by optical backscattering reflectometry measurements on a separate 2 m long spiral structure. An even lower loss of 0.8 to 0.3 dB/m over the same wavelength range has been demonstrated by the same platform, albeit with a 40 nm core thickness rather than the 100 nm found in this work [11]. The 100 nm core thickness was chosen to allow for a tighter bend radius while limiting the impact of bend loss. 7 mm die consisting of straight waveguides with facets normal to propagation and variable grating periods, lengths, and width differences were diced and tested.

Figure 1(b) gives a top down SEM micrograph of the fabricated waveguide geometry before bonding of the top thermal oxide cladding. In order to increase the contrast of the nitride to the oxide a HF dip was used to remove the partial LPCVD oxide cladding. Careful consideration of the difference between the wide and narrow waveguide sections, the width difference (highlighted by the red arrows in Fig. 1(b)), allows for control of the grating coupling constant. As is shown later, a larger grating width difference, or greater deviation from standard straight waveguide geometry, increases the modal perturbations resulting in an increased coupling constant (κ). Through the single layer sidewall geometry critical grating parameters that were before set by etch tolerances can now be more reliably controlled through nanometer scale lithographic resolution. The fabricated gratings were between 20 and

#174182 - $15.00 USD Received 10 Aug 2012; revised 15 Sep 2012; accepted 19 Sep 2012; published 10 Jan 2013

1000 µm long, with width differences between 0.4 and 4 µm, and periods of either 520 or 530 nm.

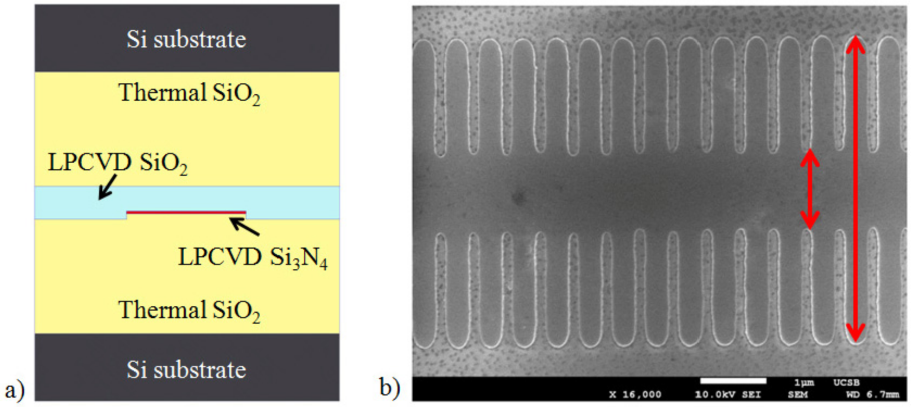

Fig. 1. (a) Schematic image of the waveguide cross section. (b) Top down SEM image of fabricated Si_3N_4 sidewall grating. Here the wide sections measure 4.6 µm in width and the narrow sections measure 1.0 µm in width. This gives a width difference of 3.6 µm. The difference of the two waveguide widths labeled by the red arrows illustrates this width difference. The period of the structure is 520 nm.

3. Grating characterization and analysis

The experimental setup used to characterize the grating spectra is shown in Fig. 2. CW output from a tunable laser was sent through a circulator to a 3-paddle polarization controller (PC) and then subsequently coupled into the grating waveguides by way of a 5 µm spot size, 25 µm working distance lensed fiber. Index matching fluid was used to improve the coupling efficiency between the lensed fiber and the diced facet. Before grating measurements were taken, the TE/TM extinction ratio of the polarization controller was measured as 15 dB. This was done at the output of the lensed fiber through the use of a free-space polarization splitter (PS) with 30 dB of extinction and a free-space Ge detector.

Light transmitted through the grating was collected with a microscope objective, passed through a polarization splitter, and focused onto an infrared camera by way of a Navitar modular zoom lens system. This allowed for quick and repeatable alignment of the input fiber to the grating waveguide. Light reflected by the grating was sent back through the circulator and detected by a broadband InGaAs photodetector. For all measurements the laser output power was set at −10 dBm across all wavelengths.

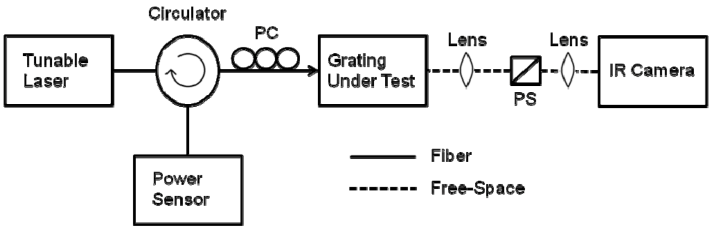

Fig. 2. Experimental setup. The tunable laser (Agilent 81680A) and power sensor (Agilent 81633A) are both housed in the same Agilent 8164A Lightwave Measurement System. The polarization controller (PC) is a 3-paddle manual polarization controller from FiberControl. The polarization splitter (PS) is a Thorlabs model CM1-PBS254 cube-mounted polarizing beamsplitter. All fibers connections are made using Corning SMF-28 fibers. The lens at the output of the grating under test before the PS is a standard 20x microscope objective.

3.1 Reflectivity spectra

Figure 3 shows the reflectivity spectrum of four separate gratings, each with a different value of width difference (which directly corresponds to the coupling constant). All of the tested grating geometries had a constant mean width ((wide section width + narrow section width)/2) of 2.8 μm. The grating reflectivity spectra exhibit the characteristic sinc function dependence that one expects for small grating perturbation values [12]. For large grating perturbation values, we measure a well-defined reflection stopband centered at 1558.3, 1557.8, and 1556.8 nm for the 1.2, 2.0, and 2.8 μm grating width differences, respectively. The shift in Bragg wavelength with increasing width difference is due to a small shift in the effective index of the mode of the periodic structure and will be discussed in Section 3.3.

The low loss (5.5 to 2.7 dB/m over the spectrum of interest) nature of the platform, coupled with the short length (7 mm) of the die, prevented us from adequately measuring the transmission spectra of the gratings. With such low loss, any unguided modes coupled into the cladding by way of the index matching fluid did not have significant distance to adequately attenuate or diverge before reaching the opposite side of the die. Neither a lensed fiber, nor the combination of a lens and a fiber collimator, could spatially filter the waveguide mode of interest from the cladding modes at the output. Once more, removal of the index matching fluid only caused the Fabry-Perot cavity created by the spacing between the lensed fibers and the chip facets to drown out the grating spectra. Because of this, we can only assume that absolute reflectivity of the gratings is given by the grating lengths and coupling constants as presented in Section 3.2. We have designed structures to measure this and will report in a future paper once we are confident of the loss of these gratings.

Of the 25 dB excess loss present in the measurement, we attribute 12 dB to extraneous system losses, such as fiber-to-fiber and fiber-to-circulator connections. This was measured through characterization of the path from the tunable laser to the lensed fiber, and from the lensed fiber to the power sensor. Since the die is of such short length, we attribute less than a dB of loss to the straight waveguide section before the gratings. This leaves two times the fiber to waveguide coupling loss (into and out of the die under test) plus the grating loss to comprise the remainder of the 13 dB excess loss present in the measurements. As discussed above we were unable to measure the transmission spectra of the gratings. Because of this we cannot say for sure the values of fiber to waveguide coupling loss, or grating loss, and again must report our findings in a future paper once we are confident of our measurements.

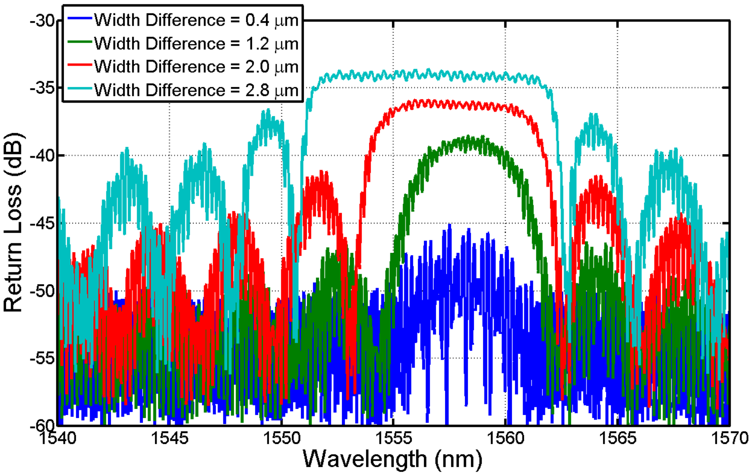

Fig. 3. Measured reflectivity spectra of four 200 μm long gratings under TE excitation. The fine oscillations are due to the 3 mm Fabry-Perot cavity created by the diced input facet and the gratings found in the center of the 7 mm chip.

3.2 Coupling constant

To analyze the behavior of such structures we turn to a coupled-mode approach. Here we express the solution to the more complex grating geometry in terms of the original basis set of eigenmodes of the simpler 2.8 μm wide straight waveguide structure. We can simplify the forthcoming analysis by first defining a set of normalized parameters [13]. We begin by defining a detuning parameter,

$$\delta = \beta - \beta_o = \frac{\omega - \omega_o}{\omega_o} \cdot \frac{\pi}{\Lambda} \cdot \frac{\bar{n}(\lambda)}{\bar{n}_{Bragg}} \tag{1}$$

where, β is the propagation constant of the waveguide, β_o is the propagation constant at the Bragg frequency ω_o (or equivalently the Bragg wavelength λ_o), $\bar{n}_{Bragg}$ is the effective index of the material specifically at the Bragg wavelength, and $\bar{n}(\lambda)$ is the effective index of the material over all wavelengths. The Bragg period of the structure, Λ, is given by

$$\Lambda = \frac{\lambda_o}{2\bar{n}}. \tag{2}$$

For waveguides containing gain or loss, β is complex, meaning that so too is the detuning parameter. It is now convenient to define a decay constant, σ, such as

$$\tilde{\sigma}^2 = \tilde{\kappa}^2 - \tilde{\delta}^2 \tag{3}$$

where the tildes are added to explicitly indicate that the coupling constant, κ, detuning parameter, δ, and decay constant, σ, can be complex. Through Eqs. (1) and (3) we can solve for the field reflectivity spectrum of the grating

$$\tilde{r}_g = -j \frac{\tilde{\kappa} \tan\mathrm{h}\, \tilde{\sigma} L_g}{\tilde{\sigma} + j\, \tilde{\delta} \tan\mathrm{h}\, \tilde{\sigma} L_g} \tag{4}$$

where L_g is the grating length. The power reflection spectrum is given by the absolute square of Eq. (4). Figure 4 plots the measured power reflectivity spectrum from a 1000 μm long grating with a width difference of 1.2 μm against the predicted spectrum as given by Eq. (4). For the theoretical spectrum it is assumed that the effective index of the material over the entire wavelength range is equal to the measured effective index at the Bragg wavelength as calculated through Eq. (2). It is this assumption that causes the peaks in the two spectra to drift slightly apart as the input light moves away from the Bragg wavelength.

With Eqs. (1) and (4) in mind, as well as the condition that power is only input into one side of the structure, the coupling constant of the grating can be approximated as one half of the reflection bandwidth. The measured bandwidths for a set of fabricated gratings are given in Fig. 5. Figure 5 also gives fitted coupling constant values for the same set of fabricated gratings. The simulated curve here is the result of a two-dimensional finite difference method numerical mode solution from the FIMMWAVE software package, which will be discussed in more detail in Section 3.3. A wide range of coupling constant values, and hence grating bandwidths, can be achieved through proper waveguide width design. For this work the width difference was varied between 0.4 and 4 μm, which yielded coupling constants from 13 to 310 cm^{-1} and grating bandwidths between 87 GHz to 2.0 THz. These values are not the limitations of the process's capability, and we expect smaller κ values to be possible through proper lithographic mask design. Such a broad range of potential κ values illustrates the wide array of applications, such as narrow linewidth mirrors, integrated pump filters, and even integrated grating-based sensors [14], made possible within this waveguide platform.

#174182 - $15.00 USD Received 10 Aug 2012; revised 15 Sep 2012; accepted 19 Sep 2012; published 10 Jan 2013
(C) 2013 OSA

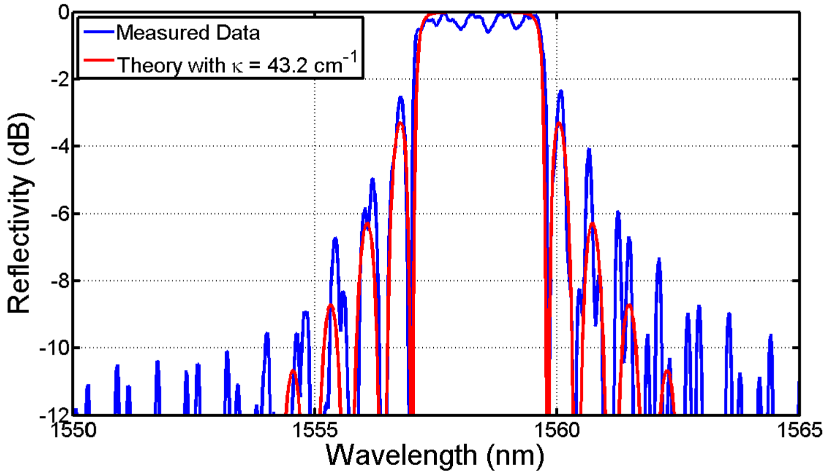

Fig. 4. Measured and theoretically predicted spectra of a 1000 µm long grating under TE excitation. Here the measured reflectivity spectrum is normalized to a maximum value of 0 dB.

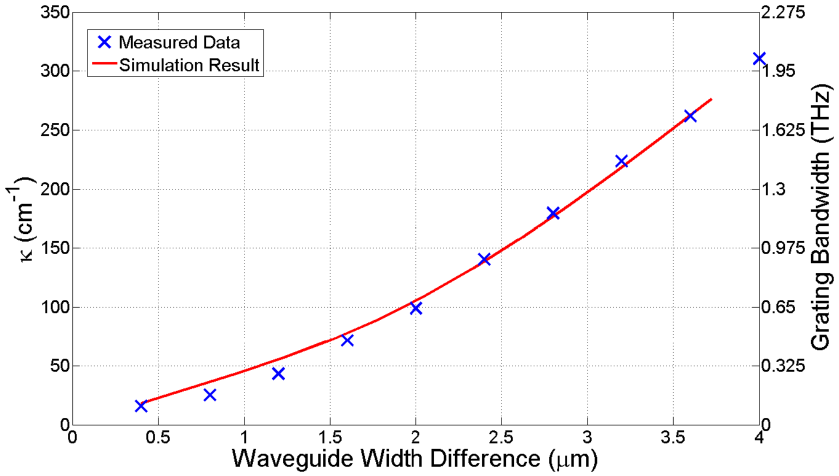

Fig. 5. Measured and simulated grating bandwidth for 1000 µm long gratings under TE excitation. The nominal waveguide width is 2.8 µm. The plot also gives fitted and simulated coupling constant values for the same set of gratings.

3.3 Duty cycle

As was shown in Fig. 3, the reflection stopband of the grating structure shifts with increasing width difference. This shift is actually quite small for such a large range of coupling constants owing to the large duty cycle of the grating. The duty cycle (DC) is defined as the percentage of the grating period occupied by the widest waveguide section. As measured in the SEM image in Fig. 1(b) the duty cycle is approximately 0.81, which may have been reduced during the BHF staining etch. Figure 6 shows the behavior of the average effective index of the grating as a function of duty cycle. As can be observed for the majority of the width differences this effective index stays close to the effective index of the unperturbed 2.8 micron straight waveguide. This graph also shows how further apodization of the duty cycle could maintain a constant effective index, and thus Bragg wavelength, across a range of coupling constants.

#174182 - $15.00 USD Received 10 Aug 2012; revised 15 Sep 2012; accepted 19 Sep 2012; published 10 Jan 2013
(C) 2013 OSA

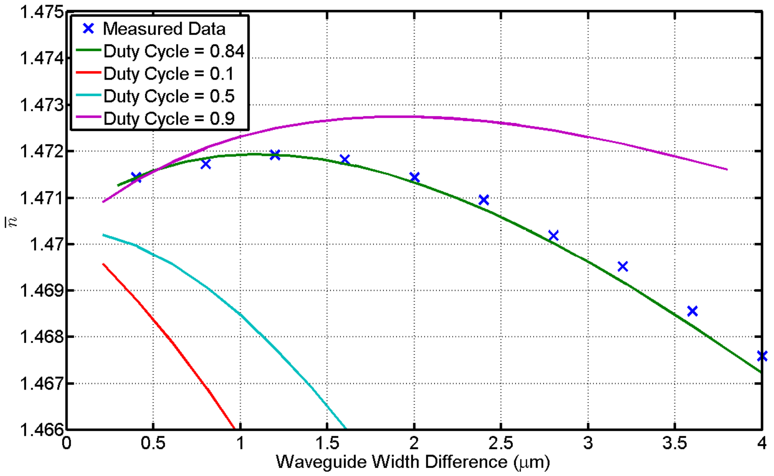

Fig. 6. Measured and predicted Bragg wavelength for different duty cycles of the sidewall geometry.

The simulations found in Fig. 6 are the result of the same FIMMWAVE script used to calculate the simulation result found in Fig. 5. Figure 7 illustrates the geometry taken into account when performing the calculations.

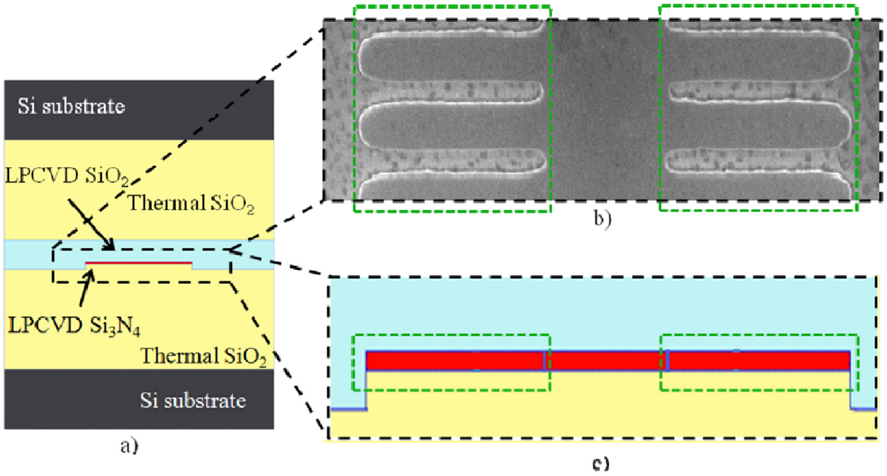

Fig. 7. (a) Cross-section, (b) top-down, and (c) on-axis view of the waveguide geometry used when performing the 2-D finite difference method simulations. The fraction of the power of the mode found within the areas defined by the green boxes (Γ) was used in the calculation of the grating coupling constant (κ) for each grating. Within the simulations it was assumed that the LPCVD SiO_2 and the thermal SiO_2 were of equivalent index value (n_{clad}).

The waveguide index profile used an approximation for the alternating SiO_2 and Si_3N_4 regions along the direction of propagation given by

$$n_{grating} = \sqrt{n_{core}{}^{2} \cdot \left(\frac{DC}{2}\right) + n_{clad}{}^{2} \cdot \left(\frac{1-DC}{2}\right)}, \tag{5}$$

where n_{core} is the refractive index of the Si_3N_4 core material and n_{clad} is the refractive index of the SiO_2 cladding material. This relationship assumes that the mode samples the near quarter-wavelength segments such that the entire mode shape is a composite of the mode in the separate wide and narrow regions of the grating. Within this single simulation we explored the variable space to make an accurate least squares fit of the duty cycle to match the data shown in Figs. 5 and 6. The coupling constant of the grating (κ) can then be found in terms of the simulation parameters as:

$$\kappa = \left(\frac{n_{grating}}{\bar{n}_{Bragg}} \right)^2 \frac{2}{\lambda} \sin(\pi \cdot DC) \cdot \Gamma \cdot (n_{core} - n_{clad}) \tag{6}$$

where Γ is the fraction of the power of the mode within the alternating wide and narrow grating regions defined by the Si_3N_4 core geometry as illustrated in Fig. 7. The sinusoidal factor is included to account for the duty cycle's influence on the grating coupling constant. Here a duty cycle of either 0 or 1 (meaning a grating where there is no width difference along its entire length) produces a coupling constant of 0, as expected of a straight waveguide. A duty cycle of 0.5 would produce the maximum value of κ for the particular width difference chosen.

4. Conclusions

We have demonstrated for the first time sidewall gratings in an ultra-low-loss Si_3N_4 planar waveguide platform. It is possible to make use of such structures for a variety of different applications, including the realization of extremely narrow linewidth mirrors. By changing the width difference between the periodic grating sections on only a single lithographic layer we can achieve coupling constants that range from 13 cm^{-1} to 310 cm^{-1}, and with careful apodization of duty cycles we can align the grating passband to match a single Bragg wavelength. The waveguide loss over the range of 1540 to 1570 nm is below 5.5 dB/m. Other interesting grating transfer functions, such as tailored spectral windows, can be achieved through use of an apodized width difference profile.

Acknowledgments

The authors thank Aurrion, Inc. for their assistance in fabricating the samples and Michael L. Davenport and John M. Garcia for useful discussions. This work was supported by DARPA MTO under iPhoD contract No: HR0011-09-C-0123. The views and conclusions contained in this document are those of the authors and should not be interpreted as representing official policies of the Defense Advanced Research Projects Agency or the U.S. Government.